

NUMERICAL STUDY OF DIRECT CONTACT CONDENSATION OF STEAM ON STABLE INTERFACE IN A BWR SUPPRESSION POOL TEST FACILITY

G. Patel*, V. Tanskanen, V. Rintala and J. Hyvärinen

LUT School of Energy Systems / Nuclear Engineering

Lappeenranta University of Technology (LUT)

PO Box 20, FIN-53851 Lappeenranta, Finland

giteshkumar.patel@lut.fi; vesa.tanskanen@lut.fi; ville.rintala@lut.fi; juhani.hyvarinen@lut.fi

ABSTRACT

The analysis of direct contact condensation (DCC) phenomena occurring in a suppression pool of BWR during steam discharge into sub-cooled water is interesting both from the numerical phase change modelling and the nuclear reactor safety points of view. This paper presents the computational fluid dynamics (CFD) simulations of a special case of low-Reynolds number DCC mode possible in suppression pools, in which the low-Reynolds number DCC corresponds to the steam. The presented CFD calculations were conducted by employing the Eulerian two-fluid approach of the OpenFOAM CFD solver. The interfacial heat transfer in these simulations was modelled by using the DCC model based on the surface divergence theory. The test STB-31 of the POOLEX facility of Lappeenranta University of Technology was used as a reference. In this test, the condensation was limited to only occur on a stable steam-water interface by applying very low steam mass flux and thermal insulation of the blowdown pipe. The results of OpenFOAM CFD solver were compared with the previously simulated results of the NEPTUNE_CFD code and with some preliminary results of the TRANSAT code. The influence of grid refinement on the DCC phenomena was assessed based on a grid convergence index. Moreover, the significance of reference bubble diameter in large interface drag modelling was studied considering various diameters. The sensitivity of sub-cooling rate on the DCC phenomenon was studied with different pool temperatures as well. The simulation results indicate that the implemented surface divergence model predicts the condensation rate quite accurately in this special case.

KEYWORDS

CFD, direct contact condensation, two-phase flow, suppression pool, interfacial area

1. INTRODUCTION

In a BWR, the suppression pool is one of the key safety systems during a loss of coolant accident (LOCA) or safety valve actuation. It provides a large pressure and heat sink by condensing vapor into liquid and absorbing the energy discharged from a reactor vessel [1]. The sub-cooling of the pool liquid and the mass flux of injected vapor determine the character of occurring direct contact condensation (DCC). By increasing mass flux, different condensation modes can be observed, varying from the DCC onto stable interfaces, through oscillatory interfaces and chugging bubbles, to condensation within quasi-steady jet interfaces. In a LOCA case, several modes will be experienced. The steam discharge into sub-cooled water is connected with hydrodynamic and thermodynamic issues like bubble dynamics, thermal stratification, mixing, steam condensation within ducts and at wall surfaces, etc. Injected steam interacts with pool water

* Corresponding author

by heat transfer, rapid condensation and momentum exchange, inducing hydrodynamic loads to the pool structures. Therefore, the proper analysis concerning steam blowdown phenomena either by experiments or with numerical simulations is of great importance from the nuclear reactor safety point of view.

Many comprehensive experimental studies with suppression pools have been reported in the literature by various injection systems both with horizontal and vertical blowdown pipes. A small review about experimental studies of suppression pool can be found from [2]. In the field of nuclear safety analysis, Computational Fluid Dynamics (CFD) has become an increasingly applicable tool for thermal-hydraulic investigations [3]. Nevertheless, the published work on the numerical simulations of the DCC phenomena in the pressure suppression pool with vertical air/steam blowdown is rather sparse. As earlier examples, the works of [4], [5] and [6] can be mentioned; they utilized the volume of fluid method for the simulations of vapor injection in water pool. The Eulerian two-fluid approach was used for the CFD modelling of chugging condensation regime by [2] and [7]. In the works of [2] and [8], the preliminary results were presented of the performance of DCC models based on the surface renewal and the surface divergence theories considering the special case corresponding the ‘oscillatory interface condensation’ mode [9] and the ‘condensation within the blowdown pipe’ mode [1].

In this paper, further analysis of that stable steam-water interface case is presented employing the Eulerian two-fluid approach of the OpenFOAM CFD solver. The standard k- ϵ turbulence model was used to model the flow turbulence. The heat transfer correlation of [10] based on the surface divergence theory was employed to model interfacial heat transfer. The steam blowdown test ‘STB-31’ of the POOLEX test facility of Lappeenranta University of Technology (LUT) and earlier NEPTUNE_CFD simulations of [2] were used as the references. In the experiment, the steam-water interface was almost flat and positioned quasi-steadily at the outlet of the blowdown pipe by virtue of very low steam mass flux applied and thermal insulation of the blowdown pipe. The paper discusses the influence of grid density on the DCC phenomena and the influence of reference bubble diameter in interface drag modelling. Furthermore, the DCC phenomena sensitivity to the sub-cooling rate is demonstrated in this paper.

2. POOLEX STB-31 EXPERIMENT

The POOLEX test facility was constructed at LUT for BWR containment studies [11]. The POOLEX test program was aimed to study and to enhance the understanding of various phenomena occurring in a BWR containment during steam discharge into sub-cooled liquid. The schematic of the POOLEX facility is shown in Fig. 1. The POOLEX facility was a cylinder shaped stainless steel pool with an open top and a conical bottom. The inner diameter of the pool was 2.4 m and the height was 5.0 m. The test facility consisted of the steam generator, the steam lines assembly, the blowdown pipe, and the water-pool. The steam generators of the Parallel Channel Test Loop (PACTEL) facility [12] were used as a steam source during the test. The steam lines from PACTEL to POOLEX facility were thermally insulated to prevent steam from condensing before being conveyed to the blowdown pipe. During test, the steam flow rate was measured with a rotameter (Krohne Model H250). There were 5 circular windows installed in the pool wall for visual observation of the interior. The details about measurement instrumentation and data acquisition can be found from [13].

A DN200 stainless steel pipe was used as a blowdown pipe which was insulated to prevent condensation on the wall, and its lower end was submerged in the water pool. The inner diameter of DN200 pipe was 0.2141 m. During the STB-31 test, the pool was filled with isothermal water and the total volume of water in this pool was approximately 12m³. The steam mass flow rate was controlled by using a manual throttle valve throughout the test to prevent steam bubble formation and to keep the steam-water interface as close as possible to the pipe outlet. Although the steam-water interface was almost smooth during the quasi-steady periods in the test, some very low amplitude oscillations were observed in the video samples. The oscillation could have originated from possible minor mechanical vibrations of the facility or from the

condensation phenomena itself. During the experiment, there were several quasi-steady state intervals suitable for the CFD validation. The experimental conditions of the STB-31 test are specified in Table I.

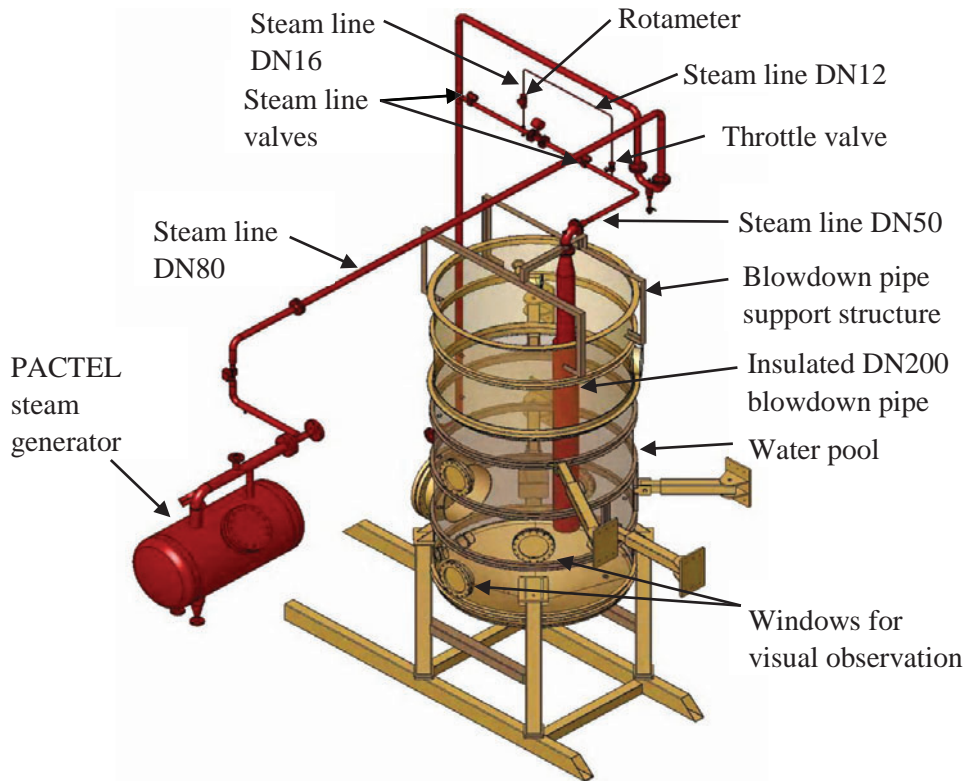


Figure 1. POOLEX test facility [13].

Table I. The test parameters of the STB-31 experiment [13].

Initial pool water level	2.95 m
Blowdown pipe submergence depth	1.81 m
Initial pool water temperature	32 °C
Steam temperature in blowdown pipe	104.35 °C
Steam pressure in blowdown pipe	0.119435 MPa
Steam flow rate	0.5...1.5 gs ⁻¹
Total duration of test	6000 s

3. MODELING AND SIMULATION STRATEGIES

3.1. Physical Models

All results presented in this paper were obtained by using the OpenFOAM CFD solver version 1.7.1. The steam-water system was simulated with the Eulerian two-fluid approach. In this approach, the interface between the phases is not tracked, because the existence of separate conservation equations for each phase does not require that. However, separate closure laws (e.g., drag, lift and added mass forces) are needed to close the equations and make the behavior of smeared interface physical. In the case of a large interface

under phase change i.e. stratified flow, the interfacial drag force and the heat/mass transfer rate are the most relevant additions needed. The transport equations of mass, momentum, and energy for two-phase flow are expressed as

$$\frac{\partial}{\partial t} (\alpha_\phi \rho_\phi) + \nabla \cdot (\alpha_\phi \rho_\phi \mathbf{U}_\phi) = \Gamma_\phi, \quad (1)$$

$$\frac{\partial}{\partial t} (\alpha_\phi \rho_\phi \mathbf{U}_\phi) + \nabla \cdot (\alpha_\phi \rho_\phi \mathbf{U}_\phi \mathbf{U}_\phi) + \alpha_\phi \nabla \cdot \boldsymbol{\tau}_\phi + \nabla \cdot (\alpha_\phi \rho_\phi \mathbf{R}_\phi) = -\alpha_\phi \nabla \bar{p} + \alpha_\phi \rho_\phi \mathbf{g} + \mathbf{M}_\phi, \quad (2)$$

$$\frac{\partial}{\partial t} (\alpha_\phi \rho_\phi H_\phi) + \nabla \cdot (\alpha_\phi \rho_\phi \mathbf{U}_\phi H_\phi) = \nabla \cdot (\alpha_\phi \rho_\phi D_{T, \text{eff}, \phi} \nabla H_\phi) + \Gamma_\phi H_{i, \phi} + Q_\phi, \quad (3)$$

where ϕ indicates an arbitrary phase (afterwards $\phi=a$ for steam and $\phi=b$ for water), α_ϕ is the phase fraction, ρ_ϕ is the density and \mathbf{U}_ϕ is the velocity of the ϕ phase. Γ_ϕ is the mass transfer rate. In Eq. (2), $\boldsymbol{\tau}_\phi$, \mathbf{R}_ϕ , $\nabla \bar{p}$, \mathbf{g} , and \mathbf{M}_ϕ denote the viscous stress tensor, the turbulent stress tensor, the overall pressure gradient, the gravity acceleration and the interfacial momentum transfer between phases, respectively. The effect of drag force was taken into account only, while the other interfacial forces were omitted in this work. The interfacial momentum exchange coefficient \mathbf{M}_{ab} can be expressed as

$$\mathbf{M}_{ab} = a_a a_b \frac{3}{4} C_{D, a} \rho_b \frac{1}{d_B} |\mathbf{U}_a - \mathbf{U}_b| (\mathbf{U}_a - \mathbf{U}_b), \quad (4)$$

where C_D is the drag coefficient which was obtained using the drag correlation of Schiller and Naumann [14], which can be written as $C_D = \frac{24}{\text{Re}_B} (1 + 0.15 \text{Re}_B^{0.687})$, and d_B is the bubble diameter. In Eq. (3), H_ϕ and $H_{i, \phi}$ indicate the specific enthalpy and the interfacial enthalpy of the ϕ phase. The terms $D_{T, \text{eff}, \phi}$ and Q_ϕ are the phase effective thermal diffusivity and the volumetric interfacial heat transfer rate, respectively. The interfacial mass transfer was calculated from the total heat balance (i.e. $Q_a + Q_b = 0$) as

$$\Gamma_{i, b} = \frac{q_a + q_b}{H_{i, a} - H_{i, b}}, \quad (5)$$

where, q_a and q_b are the sensible heat fluxes from the interface to steam and from interface to water, respectively, which can be defined as

$$q_a = a_{ia} h_{i, a} (T_{sat} - T_a), \quad (6)$$

$$q_b = a_{ib} h_{i, b} (T_{sat} - T_b). \quad (7)$$

Here a_{ia} and a_{ib} are the interfacial area densities (m^{-1}) for steam and water, respectively. The interfacial area density was calculated from the gradient of void fraction (i.e., $a_{i\phi} = |\nabla a_{i\phi}|$). The interfacial temperature, T_{sat} , was set to the saturation temperature. The terms $h_{i, a}$ and $h_{i, b}$ represent the heat transfer coefficients of steam and water. The heat transfer coefficient for the water phase can be defined as

$$h_{i, b} = \frac{\text{Nu}_b \lambda_b}{L_{t, b}}, \quad (8)$$

where Nu_b , λ_b and $L_{t, b}$ indicate the Nusselt number, the thermal conductivity and the characteristic length, respectively. In the present work, the surface divergence based DCC model of Lakehal et al. 2008 (LH) [10] was used as the water side heat transfer model. The applicability of this model has been discussed before by [2] and [8]. In the DCC model, Nu_b is defined as

$$\text{Nu}_b = Bf [\text{Re}_t^m] \text{Re}_t \text{Pr}^{1/2}. \quad (9)$$

B is the model constant (i. e., $B = 0.35$ for $\text{Pr} \approx 1$ and $B = 0.45$ for $\text{Pr} \gg 1$; here, $B=0.35$ was used) and $f [\text{Re}_t^m]$ can be written as

$$f [\text{Re}_t^m] = \left[0.3 \left(2.83 \text{Re}_t^{3/4} - 2.14 \text{Re}_t^{2/3} \right) \right]^{1/4} \text{Re}_t^{-1/2}. \quad (10)$$

Here, $\text{Re}_t = \frac{k_b^2}{v_b \varepsilon_b}$, where, k_b , ε_b , and v_b are the turbulence kinetic energy (TKE), the dissipation rate of TKE, and the kinematic viscosity of water. In Eq. (8), $L_{t,b} = \frac{v_b}{u_t} \text{Re}_t$, where, the velocity parameter, u_t , was defined as $u_t = (v_b \varepsilon_b)^{1/4}$. Flow turbulence was solved by employing the standard $k-\varepsilon$ turbulence model of [15]. In the present work, the transport equations of turbulence model were solved for one continuous phase only (i.e., water), while the ‘dispersed’ phase (i.e., steam) turbulent viscosity and turbulent kinetic energy were the continuous phase values scaled with the turbulence response coefficient. In NEPTUNE_CFD simulations, the liquid phase turbulence was solved by the standard $k-\varepsilon$ model while the vapor phase was treated as a laminar flow. TransAT was applied as a single fluid solver i.e. using Level-Set method for two phase flow and turbulence was modeled by the standard $k-\varepsilon$ turbulence. Therefore these codes solve the interfacial turbulence differently at least to some extent. However, in this stable interface case, the differences in drag modelling and interfacial area modelling influenced more than the differences in the turbulence modelling.

3.2. Numerical Details

3.2.1. Geometrical details and simulation set up

In order to solve the case as 2D-axisymmetric one with a 3D solver, all of the presented numerical results of this study were simulated using a 1° sector of the POOLEX pool. Therefore, a 2D-axisymmetric grid of hexahedral cells was generated by rotating a quadrilateral grid to contain a single cell thickness in respect to z-axis. The total radius and the height of the computational domain was set to 1.2 m and to 2.63 m, respectively. By using this height, the initial surface of water could be set on the upper edge of the domain. Moreover, the lower conical part of the test vessel was truncated off at 0.8 m from the mouth of the blowdown pipe. The computational grid for the simulation is presented in Fig. 2.

In the case of STB-31 test, the location of the steam-water interface was almost stationary at the blowdown pipe mouth. Therefore, the grid was more refined near the pipe mouth. A grid independence study was performed considering four different grid, i.e., Grid A (2500 cells), Grid B (6270), Grid C (14014), and Grid D (20940). The minimum cell sizes in the refined region of Grid A, B, C and D were circa 0.1×6 mm, 0.03×3 mm, 0.006×0.6 mm and 0.001×0.2 mm, respectively. In the STB-31 test, the inlet steam mass flow rate was very small. Therefore, the velocities within the calculation domain remained low. However, the wall function approach of $k-\varepsilon$ turbulence model ($y^+ > 30$ preferred) would lead to a notably coarse calculation grid relative to the interface and condensation modelling. Therefore, the grid densities near to the blowdown pipe wall were high i.e. $y_{\text{Grid A}}^+ \approx 5.3$, $y_{\text{Grid B}}^+ \approx 1.9$, $y_{\text{Grid C}}^+ \approx 0.6$, and $y_{\text{Grid D}}^+ \approx 0.1$. The discretization error, the main source of computational errors, can be defined as the difference between the exact solution of the governing equations and the discretized system. These errors can arise from numerical algorithms, the grid structure and/or quantity, boundary conditions, etc. In the present work, the errors resulting from the number of grid points are discussed. The study of the grid refinement influence on the CFD results was performed by using the grid convergence index (GCI) method. The GCI method proposed by Celik et al. [16] was used. This method is based on the Richardson extrapolation technique [17], in which

multiple solutions of the numerical calculation are calculated by adjusting a parameter (grid size) and are used then to extrapolate a more accurate solution. The grid convergence was evaluated by using a relative error measure of different parameters between the grids as $e_a^{nm} = \left| \frac{\Phi_n - \Phi_m}{\Phi_n} \right|$. Here Φ_n and Φ_m denote the corresponding solutions of n^{th} and m^{th} grid, respectively. An extrapolated relative error was calculated as $e_{ext}^{nm} = \left| \frac{\Phi_{ext}^{nm} - \Phi_n}{\Phi_{ext}^{nm}} \right|$, where, Φ_{ext}^{nm} is the extrapolated value which can be defined as $\Phi_{ext}^{nm} = \frac{r_{nm}^p \Phi_m - \Phi_n}{r_{nm}^p - 1}$. Here, r_{nm} represents the grid refinement factor which can be evaluated from the ratio of corresponding grid sizes of n and m grids, and p indicates the order of the discretization method. More details of the procedure to estimate the discretization error can be found from [16].

The GCI provides a uniform measure of convergence for grid refinement tests. The GCI can be estimated as

$$GCI^{nm} = F_s \frac{e_a^{nm}}{r_{nm}^p - 1}. \quad (11)$$

Here, F_s is the safety factor, which was 1.25. This value is based on the experience obtained by applying GCI to many situations [18]. Furthermore, the theory of Richardson extrapolation and therefore of the proposed GCI depends on the assumption that the Taylor series expansion is valid asymptotically and the two grids are within the asymptotic range. The asymptotic range of convergence between grids can be achieved as

$$GCI^{23} = r_{nm}^p GCI^{12}. \quad (12)$$

Here, superscripts 12 and 23 indicate from fine to intermediate and from intermediate to coarse grid refinements, respectively. The influence of grid density and the grid discretization error is discussed in Section 4.

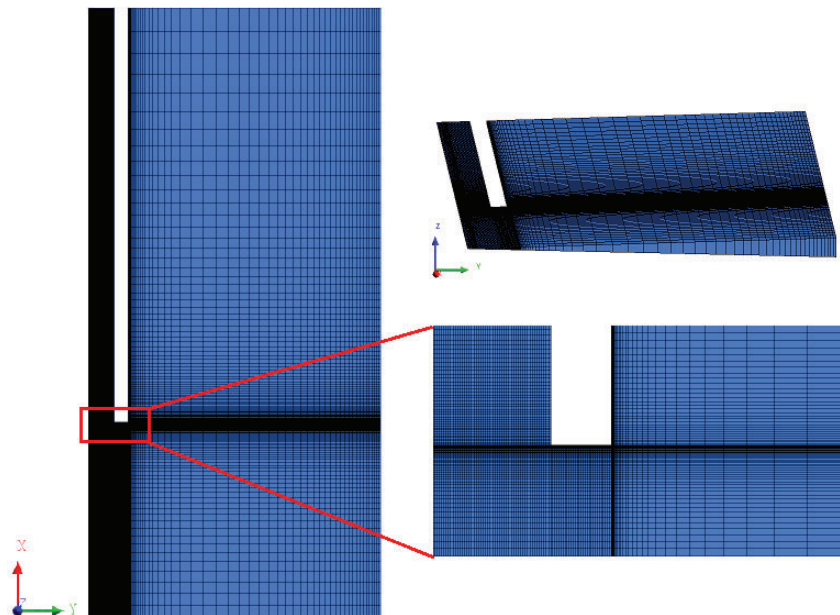


Figure. 2. The 2D-axisymmetric grid of the POOLEX pool.

The CFD simulations of this work were performed with the finite volume formulation. The pressure in the water volume was initialized by using the hydrostatic pressure. The pressure and the temperature fields of

the steam were initialized according to the STB-31 test conditions (Table I). The water surface as the upper boundary of the computational domain was fixed to the atmospheric pressure of 0.10287 MPa. Moreover, the steam was assumed to be approximately at the saturated state. Initially, the turbulent kinetic energy and its dissipation rate fields in the pool-water were initialized with generic 10^{-4} and 10^{-3} , respectively. The pool walls were considered to be adiabatic and no-slip boundary conditions were imposed on all the wall surfaces. Reliable modelling of non-condensable gases fraction and its effects would be a notable additional challenge in the CFD simulations. Thus, the effect of non-condensable was omitted in the CFD simulations. The uncertainties due to the non-condensable gases in the STB-31 test are discussed in [2], in which he applied the Couette flow film model of [19] to produce an estimation of the non-condensables effect on the condensation rate during the selected period of the experiment. His analysis was based on the air and steam partial pressures derived from the measured temperatures and the total pressure at the outlet of the pipe. The analysis indicated that 3–50 % higher condensation rates would occur without the presence of non-condensable gases. The solution methodology was based on incompressible formulation of OpenFOAM. The pressure-velocity coupling was done using the PIMPLE algorithm which is a combination of PISO and SIMPLE algorithms. A velocity boundary condition was set to the blowdown pipe inlet for the steam phase. Based on the selected quasi-steady period in the STB-31 experiment, the inlet velocity of 0.043 ms^{-1} was used corresponding to the mass flow rate of 1.0594 gs^{-1} . A 2nd order upwind discretization scheme was employed for the phase volume fraction, the phase velocities, and the turbulent kinetic energy and its dissipation rate. The normalized RMS residuals of the order of 10^{-4} or lower were used as convergence criteria. Simulations were performed with the fixed time step size of 0.1 ms for the total time span of 15 s.

4. RESULTS AND DISCUSSION

The total duration of the STB-31 experiment was about 6000 s containing several quasi-steady state intervals in which the steam-water interface was almost stable at the blowdown pipe mouth. A 300 s period (from 2014 s to 2340 s) from the STB-31 experiment was selected as reference for the CFD simulations. Firstly, the influence of computational grid density on DCC phenomena was studied based on four different grid sizes. Fig. 3 shows the steam volume fraction field near the blowdown pipe mouth predicted with different grids. It is observed that the coarser grid (Grid A) resulted in visibly more smeared steam-water interface compared to the other grids. As the grid density increases, the interface profile becomes sharper. The sharpest interface was captured by the finest grid (Grid D). Based on these qualitative results, it was essential to investigate the influence of grid density to the convergence of the DCC phenomena.

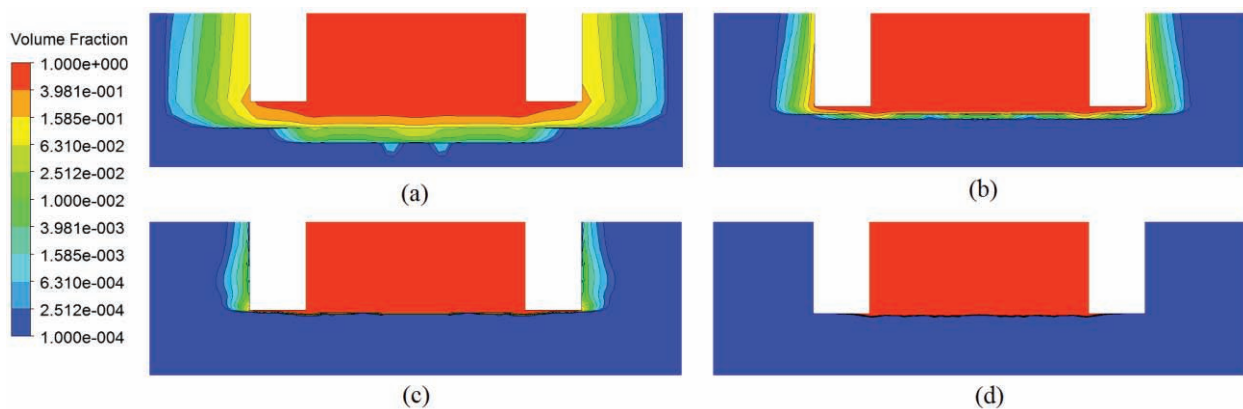


Figure 3. Volume fraction fields predicted by (a) Grid A, (b) Grid B, (c) Grid C, and (d) Grid D near blowdown pipe mouth in a 2D-axisymmetric OpenFOAM simulation of the STB-31 test.

The DCC rate cannot be measured easily in the blowdown experiments. In the STB-31 test, the steam mass flow rate was controlled through the experiment to prevent steam bubble formation and to keep the steam-water interface as close as possible to the blowdown pipe outlet. Therefore, it could be assumed that the injected steam mass flow rate was almost equal to the condensation mass flow rate itself. Based on this assumption, it was possible to compare the test and simulation results of the DCC rates. Fig. 4 presents the predicted condensation mass flow rate, the condensation mass flux, and the total interfacial area with different grids. The CFD results are compared to the measured data of the STB-31 test. The relatively high measurement error in the condensation mass flow rate is not displayed in the figure. The range of measurement error was $\pm 1.3 \text{ gs}^{-1}$. In the grid independence test simulations, the steam-water interface was initialized 5 cm inside from the blowdown pipe outlet at $t = 0$. The steam-water interface starts to approach to the blowdown pipe mouth as simulation time elapsed. It took about 5 s of simulation time to reach to the blowdown pipe mouth. Therefore, for all the cases, the condensation mass flow rate was lower than the STB-31 inlet flow rate at the beginning of the simulations as shown in Fig. 4(a). The Grid A produced clearly weaker condensation rate than the others. As the grid density increased, the predicted condensation mass flow rate reached to the measured value. Grid C and Grid D yielded to relatively similar and accurate results of the DCC rate. The condensation mass flow rate includes the effect of interface area fluctuations during the simulations. Because the interfacial area changes due to the interface fluctuation, that have an effect on the total condensation rate. For this reason, it was essential to present also the interfacial mass fluxes (Fig. 4(b)) by dividing the total DCC rates by the total interfacial areas (Fig. 4(c)).

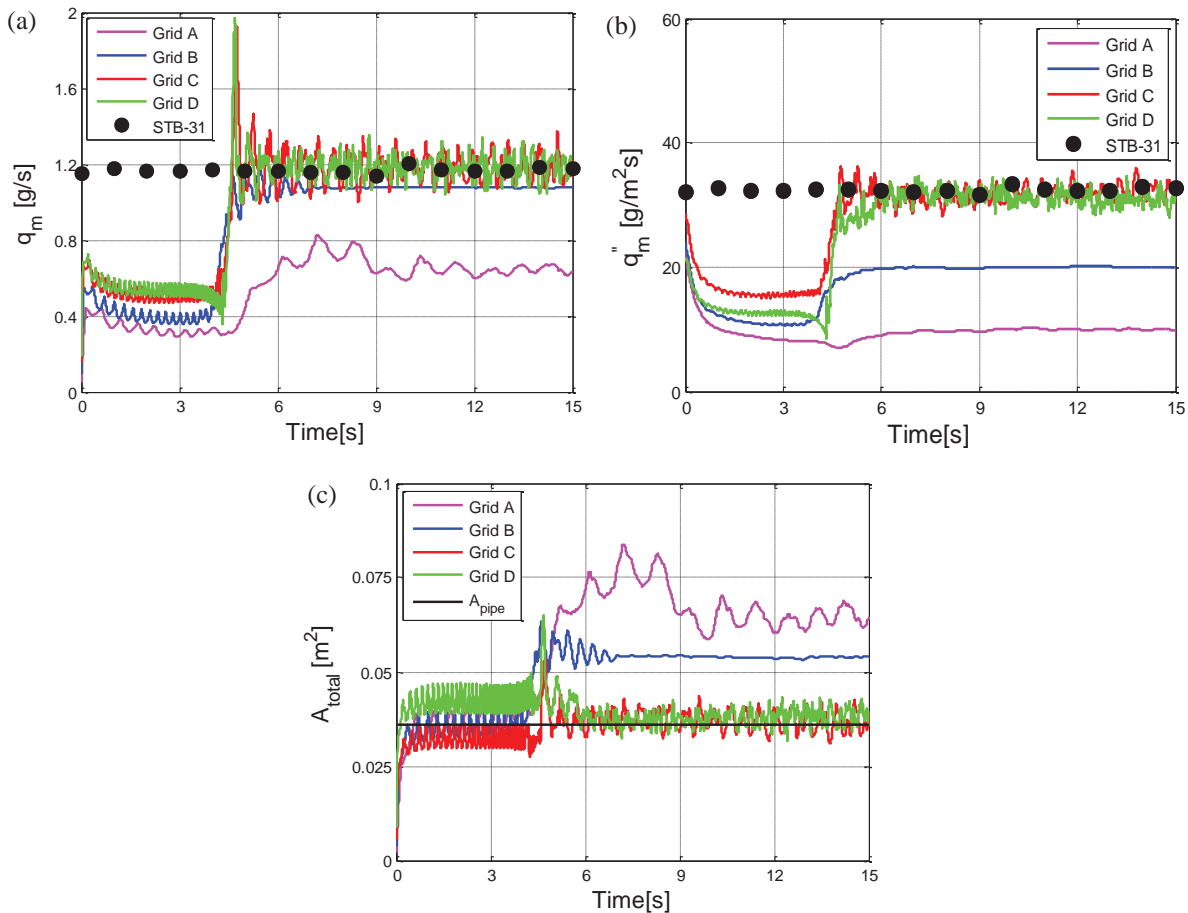


Figure 4. Predicted (a) condensation mass flow rate, (b) condensation mass flux, and (c) total interfacial area by the LH model using OpenFOAM versus the STB-31 test data. A_{pipe} indicates the cross-sectional area of the blowdown pipe outlet in the STB-31 test.

As presented in Fig. 4(b), the Grid A and Grid B strongly underpredicted the condensation mass flux, while the Grid C and Grid D predicted the condensation mass flux very close to the measurements. The interfacial area should be close to the cross-sectional area of pipe outlet. Grid A and Grid B over predicted the total interfacial area by 140-150 % and 170-200 % of the cross-sectional area of the outlet, respectively. The Grid C and Grid D produced better results. However, in both the Grid C and Grid D case, slight wavy-motions of the steam-water interface occurred. Possible mechanical vibrations were not modeled in the CFD simulation. Therefore, the oscillating wavy interfacial motion appears likely due to an instability in the total DCC rate. The instability in total DCC rate occurs probably because the DCC rate in the smooth free surface area could be lower than the amount of injected steam, which forces the steam to spread onto the wall of the pipe lip where the condensation rate increases. The 2D-axisymmetric geometry enhances this effect.

The GCI method was used to calculate the discretization error for the CFD simulations with selected grid refinements. Table II summarizes the discretization errors for the condensation mass flow rate and the total interfacial area. The Cases AB, BC and CD indicate the grid refinements from Grid A to B, Grid B to C, and Grid C to D, respectively. It can be seen that the calculated relative error (i.e., e_a) decreased as the grid density increased. Moreover, the successive grid refinements resulted in a reduction for an extrapolated relative error (i.e., e_{ext}) as well. The GCI value for the successive grid refinements reduced well for both the quantities. The GCI values indicate that the grid refinement from Grid C to Grid D yielded a negligible discretization numerical error which was less than 0.1 %. Furthermore, the asymptotic range of convergence has been calculated. For the grid group of A, B and C, the asymptotic range of convergence for condensation mass flow rate and total interfacial area are 1.04448 and 1.09235, respectively and for the grid group of B, C and D, the asymptotic range of convergence for condensation mass flow rate and total interfacial area are 1.00569 and 1.00238, respectively. This analysis shows that the asymptotic range of convergence for the grid groups are approximately unity, which indicates that the solution is well within the asymptotic range of convergence. Based on this analysis, the finest grid, Grid D was selected for the further calculations.

Table II. Details of the grid discretization error.

Quantity	Error (%)	Case AB	Case BC	Case CD
Condensation mass flow rate	e_a	60.82	12.00	0.52
	e_{ext}	19.04	1.48	0.07
	GCI	47.27	2.10	0.09
Total interfacial area	e_a	15.30	26.89	0.84
	e_{ext}	29.25	2.30	0.05
	GCI	23.95	2.05	0.06

Also, the results of Grid D of OpenFOAM code were compared with the previously simulated results of the NEPTUNE_CFD of [2]. During the STB-31 test, it was noticed that there were non-condensing bubbles (air bubbles) escaping around the pipe lip. Therefore, it was assumed that dissolved air was released from the pool water, and it slowly accumulated as a layer between steam and water inside the blowdown pipe. In order to mitigate the non-condensable gases effect on the condensation rate, it was essential to remove the layer of air from the blowdown pipe. That was done by increasing the steam flow rate at certain time intervals. Therefore, during STB-31 test, the steam mass flow rate at inlet was increased at regular time periods (e.g., during 1185...1525 s, 2455...2830 s, and 3800...3950 s). After such a strong blowdown, steam mass flow rate was decreased to attain stable interface conditions again. Fig. 5(a) displays video frames of stable interface (left) and strong blowdown (right) during the STB-31 POOLEX test. Fig. 5(b) and (c) compare the contours of steam volume fraction and turbulent kinetic energy weighted by volume fraction of water of OpenFOAM and NEPTUNE_CFD, respectively. It can be seen that both the CFD solvers predicted well the profile of the steam-water interface. The turbulence kinetic energy and therefore

the DCC rate at the outer surface and at the lip area of the pipe seem to be higher in the OpenFOAM simulation than in the NEPTUNE_CFD case. This may occur due to the bit higher residual bubble escape around the pipe mouth in the OpenFOAM case. However, the higher interfacial turbulence kinetic energy in the NEPTUNE_CFD case indicates that there are differences in the modelling of interfacial turbulence between the codes as well. In both the codes, the standard k- ϵ formulation and standard no-slip boundary conditions may yield local mispredictions in the near wall turbulence values as well. Higher interfacial turbulence in the NEPTUNE_CFD case may reduce the amount of escaping steam around the pipe lip reducing therefore the turbulence on the lip wall region as well.

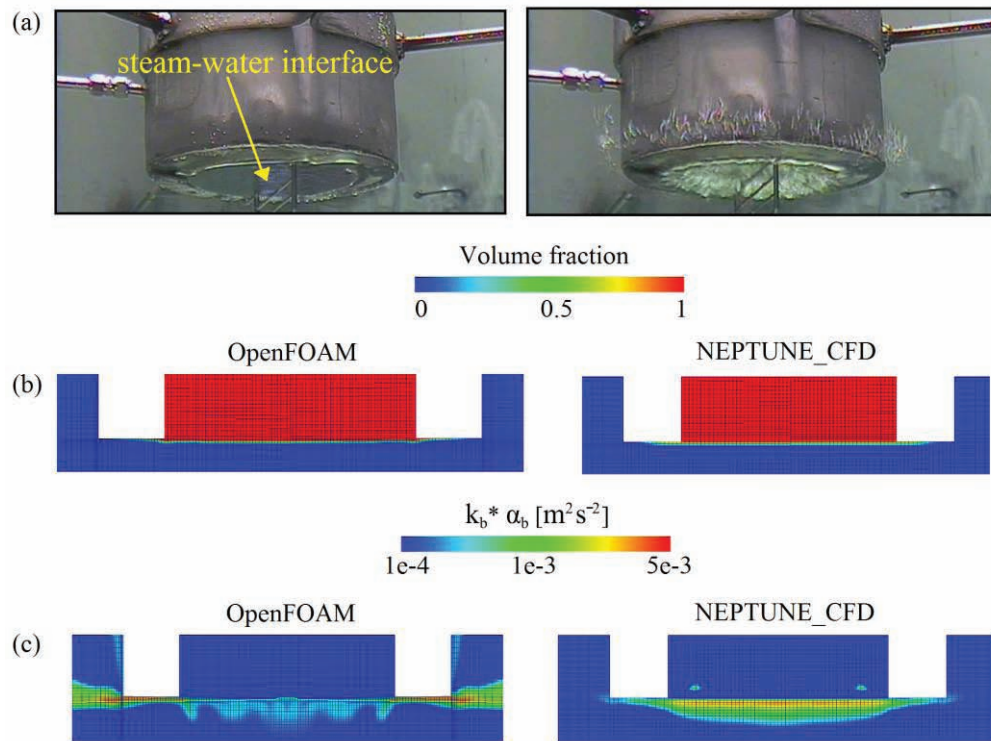


Figure 5. (a) Instantaneous images of stable steam-water interface (left) and strong blowdown of steam (right) during STB-31 POOLEX test, (b) contours of the steam volume fraction, and (c) the water phase turbulence kinetic energy times phase fraction of water near blowdown pipe mouth in 2D-axisymmetric simulations of STB-31 test with the OpenFOAM and NEPTUNE_CFD.

Furthermore, the predicted condensation mass flow rate of OpenFOAM was compared with the NEPTUNE_CFD and also the preliminary TransAT results of [2] in Fig. 6. Concerning reliable comparison, the available TransAT transient is too short compared to OpenFOAM and NEPTUNE_CFD simulations. The solid black lines indicate the measurement error range of the measured steam flow rate during STB-31 test. In this case, the steam-water interface was initialized exactly at the blowdown pipe outlet. The OpenFOAM simulation predicted the condensation mass flow rate almost to the measured values. The NEPTUNE_CFD simulations were conducted by using a pressure boundary condition at inlet and steam tables, whereas the OpenFOAM simulations were carried out by using the velocity inlet boundary condition and constant steam properties. These differences resulted in slightly different interfacial behavior which was a probable reason for the 50 % overestimation in the condensation mass flow rate results by NEPTUNE_CFD compared to the OpenFOAM and measurements. Although the condensation rate in the TransAT case is higher than in the other cases, the order of magnitude is same, which is not obvious in DCC simulations with different methods and computational grids. The TransAT grid was almost two times

denser than the OpenFOAM and NEPTUNE_CFD ones. Moreover, the TransAT code version was an interface tracking method code (Level-Set) using constant material properties. Regardless of the differences in the DCC rates of the codes, all the results fall quite well between the measurement error bounds.

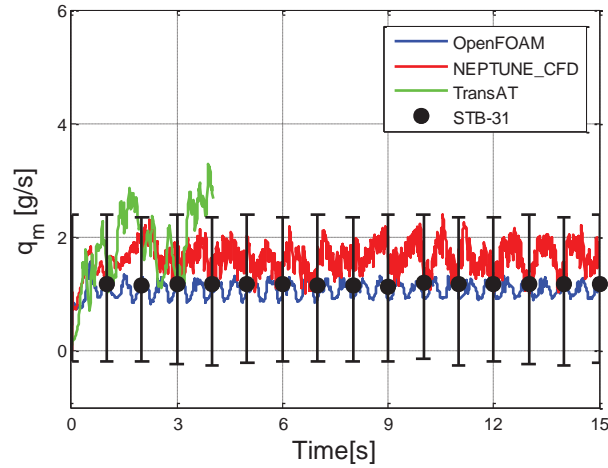


Figure 6. Predicted condensation mass flow rate by the LH model using OpenFOAM, NEPTUNE_CFD and TransAT versus the STB-31 experimental data.

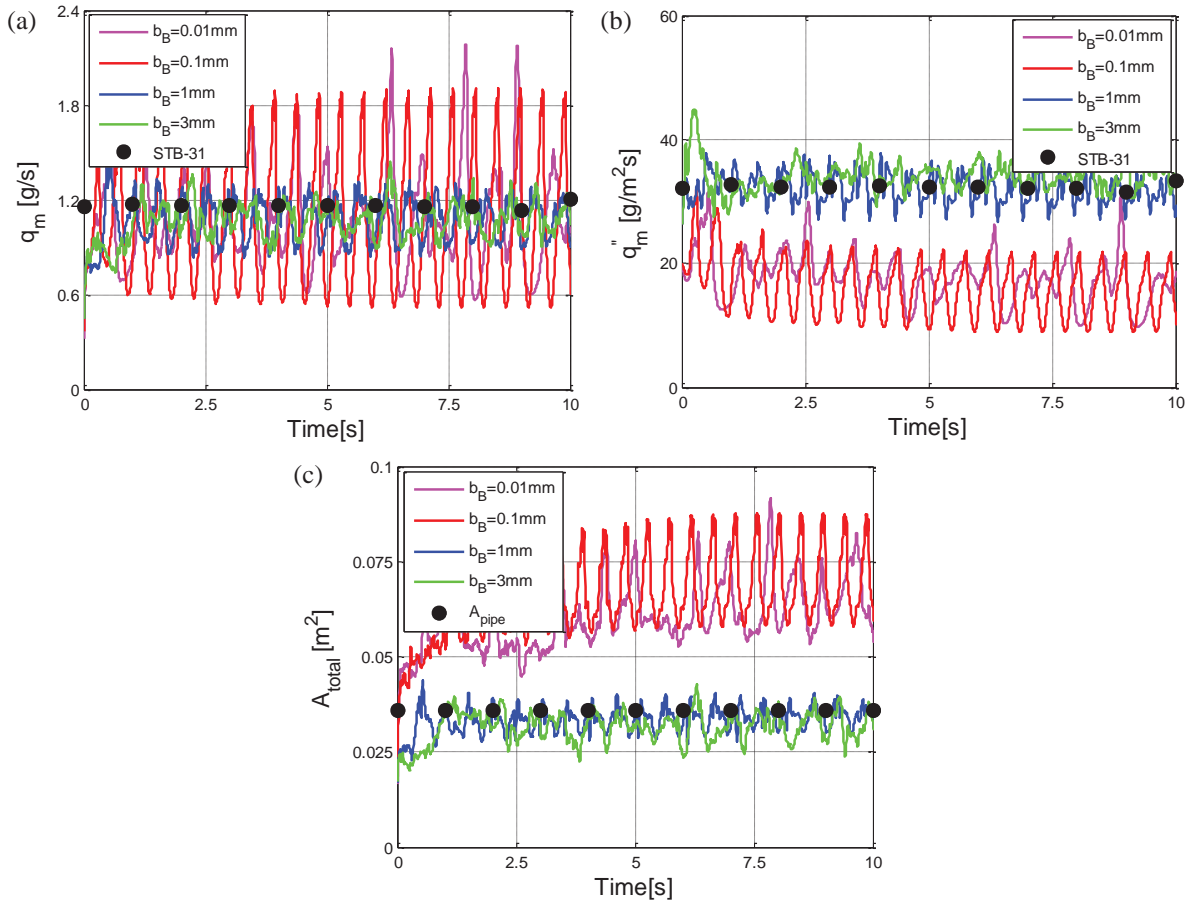


Figure 7. Predicted (a) condensation mass flow rate, (b) condensation mass flux, and (c) total interfacial area with different bubble sizes using OpenFOAM versus the STB-31 test data.

The influence of reference bubble diameter of the steam phase on the DCC rate in large interface drag modelling by the Schiller-Naumann drag coefficient was studied by testing various diameters. Four reference bubble diameters were considered, i.e., 0.01 mm, 0.1 mm, 1 mm and 3 mm. The corresponding results are presented in Fig. 7. The smaller bubble diameter cases (i.e., $d_B = 0.01$ mm and 0.1 mm) yielded higher interfacial area than the bigger bubble diameter cases (Fig. 7(c)). Therefore, the enlarged interfacial area increases the total DCC rate locally (Fig. 7(a)). However, in the case of $d_B = 0.01$ mm and 0.1 mm, the condensation mass flux is decreased more than 50 % in turn (Fig. 7(b)). It can be seen that the profiles of condensation mass flow rate, condensation mass flux and total interfacial area with $d_B = 1$ mm and 3 mm are quite near to the measured values. As the modeled case operates in clearly separated flow regime, the reference diameter in the bubbly flow drag coefficient in the interfacial momentum transfer model turns out as a fitting parameter.

The influence of sub-cooling rate on the DCC phenomena was studied with different pool temperatures (i.e., $T_b = 288.15$ K, 308.15 K and 328.15 K). Fig. 8(a) demonstrates that the condensation mass flow rate was decreased as the pool temperature increased. The cold temperature in the interface region increases the condensation rate and, therefore, the total interfacial area decreases due to rapid phase change (Fig. 8(c)). Due to lower DCC rate (i.e., condensation mass flux) in the case of $T_b = 328.15$ K, the interfacial area increases. Although the effect of pool sub-cooling on the DCC rate is quite obvious, it is essential to see of how easily it changes the behavior of the interface in certain geometries such as the blowdown pipe outlet.

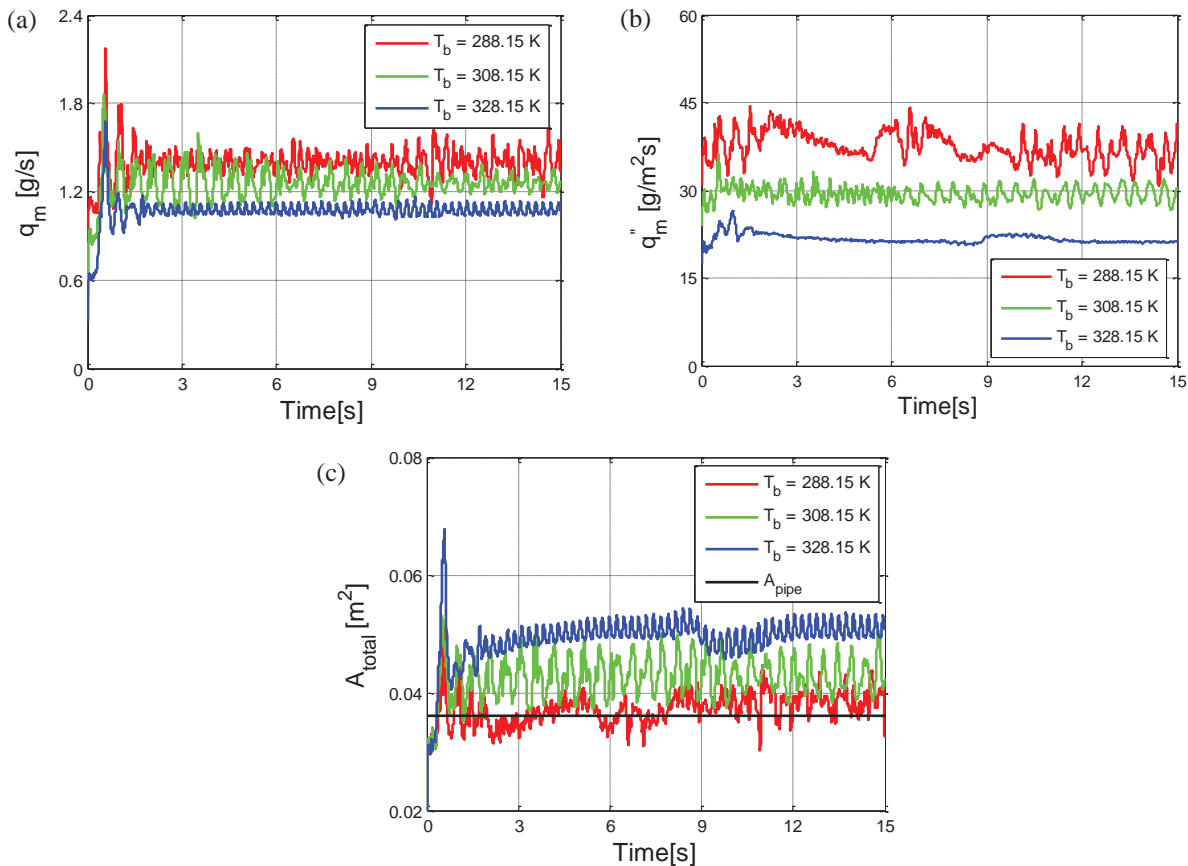


Figure 8. Predicted (a) condensation mass flow rate, (b) condensation mass flux, and (c) total interfacial area with different pool water temperatures by the LH model using OpenFOAM.

5. CONCLUSIONS

In this study, a CFD analysis of DCC of steam was conducted by using the Eulerian two-fluid approach of the OpenFOAM CFD solver. A special case of relatively low-Reynolds number (i.e., about 500 corresponding to the steam injection blowdown pipe diameter) DCC mode possible in suppression pools of BWRs was modelled, in which the steam-water interface was flat and positioned quasi-steadily at the outlet of the blowdown pipe. The surface divergence theory based DCC model of [10] was employed to estimate the interfacial heat transfer in the simulations. As the reference, the steam blowdown test 'STB-31' of the POOLEX test facility of Lappeenranta University of Technology was used. The simulated results of the OpenFOAM CFD solver were discussed together with previously simulated results of NEPTUNE_CFD of [2] and a short sample of results obtained with TransAT of [2]. In the STB-31 test, the steam mass flow rate was controlled to prevent steam bubble formation and to maintain the steam-water interface position stationary as close as possible to the blowdown pipe outlet. Therefore, it was assumed that the injected steam mass flow rate was almost equal to the condensation mass flow rate itself.

Firstly, the influence of computational grid refinement on the DCC phenomena was investigated via grid convergence index analysis. The predictions of the condensation mass flow rate and the total interfacial area were sensitive to the grid refinements. However, it can be concluded that adequate grid density (i.e., the grid which contained the minimum cell dimensions approximately 0.001 mm and 0.2 mm in horizontal and vertical directions, respectively) was achieved to obtain correct rate of DCC in this low-Reynolds number DCC case. The qualitative and quantitative behavior of the steam-water interface agreed well to the test results in the simulations with the OpenFOAM and NEPTUNE_CFD CFD solvers. However, mild oscillatory and wavy behavior of interface was recognized in the OpenFOAM simulations. In the DCC model used, the DCC rate is dependent on the turbulence kinetic energy. Therefore, the observed oscillations in the OpenFOAM simulations can be described by the difference in the turbulence kinetic energy between the pipe lip, outer surface and free interface regions. In the OpenFOAM simulations, a small amount of steam escaped occasionally nearby the pipe lip, which raised local interfacial shear and consequently turbulence kinetic energy as well. Also, the influence of reference bubble diameter of steam in interfacial drag modelling on the DCC phenomena was studied. The interfacial drag coefficient suitable for bubbly flow was used for separated flow by adjusting the reference bubble diameter. Results indicated that by trying a very small bubble diameter also the condensation mass flux can be affected i.e. become underestimated significantly. The sensitivity of sub-cooling rate on the DCC phenomena was studied with different pool temperatures as well. The effect of pool sub-cooling on the DCC rate was notable even in the mild condensation case of almost flat steam-water interface.

The presented CFD results provide motivation for further condensation model validation and development work particularly for more vigorous and challenging condensation modes of steam blowdown appear in suppression pools of BWRs.

ACKNOWLEDGMENTS

The research leading to these results was funded by the Finnish Nuclear Waste Management Fund (VYR) via The Finnish Research Programme on Nuclear Power Plant Safety SAFIR2014 and the Academy of Finland via the Doctoral Programme for Nuclear Engineering and Radiochemistry (YTERA). The research leading to NEPTUNE_CFD and TransAT results is partly funded by the European Atomic Energy Community's (Euratom) Seventh Framework Programme FP7/2007-2011 under grant agreements No. 232124 and No. 323263. The authors gratefully acknowledge this support.

REFERENCES

1. R. Lahey and F. Moody, “*Thermal-Hydraulics of a Boiling Water Reactor*,” 2nd edition, Chapter 11, American Nuclear Society, USA (1993).
2. V. Tanskanen, “CFD modelling of direct contact condensation in suppression pools by applying condensation models of separated flow,” *Acta Universitatis Lappeenrantaensis 472. Lappeenranta University of Technology*. ISBN 978-952-265-221-8, ISBN 978-952-265-222-5, Ph.D. thesis, ISSN 1456-4491 (2012).
3. D. Bestion, “Applicability of two-phase CFD to nuclear reactor thermalhydraulics and elaboration of best practice guidelines,” *Nucl. Eng. Des.*, **253**, pp. 311-321 (2013).
4. M. Meier, G. Yadigaroglu and M. Andreani, “Numerical and experimental study of large steam-air bubbles injected in a water pool,” *Nucl. Sci. Eng.*, **136**, pp. 363-375 (2000).
5. G. Yadigaroglu, “Computational Fluid Dynamics for nuclear applications: from CFD to multi-scale CMFD,” *Nucl. Eng. Des.*, 235, pp. 153-164 (2004).
6. R. Thiele, “Modeling of direct contact condensation with OpenFOAM,” *Division of Nuclear Reactor Technology, Royal Institute of Technology, KTH*, Stockholm, Sweden. Master thesis, ISSN 0280-316X (2010).
7. V. Tanskanen, A. Jordan, M. Puustinen, and R. Kyrki-Rajamäki, “CFD simulation and pattern recognition analysis of the chugging condensation regime,” *Annals of Nuclear Energy*, **66**, pp. 133-143 (2014).
8. G. Patel, V. Tanskanen and R. Kyrki-Rajamäki, “Numerical modelling of low-Reynolds number direct contact condensation in a suppression pool test facility,” *Annals of Nuclear Energy*, **71**, pp. 376-387 (2014).
9. C. Chan and C. Lee, “A regime map for direct contact condensation,” *Int. J. Multiphase Flow*, **8**, pp. 11-20 (1982).
10. D. Lakehal, M. Fulgosi and G. Yadigaroglu, “DNS of Condensing Stratified Steam Water Flow,” *ASME J. Heat Transfer* **130**, 021501-10 (2008).
11. M. Puustinen, R. Kyrki-Rajamäki, V. Tanskanen, A. Räsänen, H. Purhonen, V. Riikonen, J. Laine and E. Hujala, “BWR suppression pool studies with POOLEX and PPOOLEX test facilities at LUT,” in: The 15th International Topical Meeting on Nuclear Thermal Hydraulics (NURETH-15), Pisa, Italy, May 12-17 2013, pp. 1-12 (2013).
12. J. Tuunanen, J. Kouhia, H. Purhonen, V. Riikonen, M. Puustinen, R. S. Semken, H. Partanen, I. Saure and H. Pylkkö, “General description of the PACTEL test facility,” *VTT Research Notes 1929*, VTT, Finland, ISBN 951-38-5338-1 (1998).
13. J. Laine and M. Puustinen, “Condensation Pool Experiments with Steam using Insulated DN200 Blowdown Pipe,” *Research Report POOLEX 3/2005*. Lappeenranta University of Technology, Lappeenranta, Finland (2006).
14. L. Schiller and A. Naumann, “Über die grundlegenden Berechnungen bei der Schwerkraftbereitung,” *Z. Verein Deutscher Ing.* **77**, pp. 318-320 (1933).
15. B. E. Launder and B. I. Sharma, “Application of the energy dissipation model of turbulence to the calculation of flow near a spinning disc,” *Letters in Heat Mass Transfer*, **1**, pp. 131-138 (1974).
16. I. B. Celik, U. Ghia, P. J. Roache, C. J. Freitas, H. Coleman, and P. E. Raad, “Procedure for estimation and reporting of discretization error in cfd applications,” *J. Fluids Eng.*, **130** (7), 1-4 (2008).
17. L. F. Richardson and J. A. Gaunt, “The deferred approach to the limit,” *Philos. Trans. Roy. Soc. London. Ser. A*, **226**, pp. 299-361 (1927).
18. P. J. Roache, “Perspective: A method for uniform reporting of grid refinement studies,” *J. Fluids Eng.*, **116**, pp. 405-413 (1994).
19. S. Ghiaasiaan, “*Two-Phase Flow, Boiling and Condensation in Conventional and Miniature Systems*,” 1st edition, Cambridge University Press, New York, ISBN 978-0-521-88276-7 (2008).